

Interfacial Alignment Mechanism of Forming Spherical Silica with Radially Oriented Nanopores

Bing Tan and Stephen E. Rankin*

Chemical and Materials Engineering Department, University of Kentucky,
177 Anderson Hall, Lexington, Kentucky 40506-0046

Received: August 9, 2004; In Final Form: October 8, 2004

When cationic surfactants are added to the Stöber process, spherical particles with radially oriented mesopores can be prepared by precipitation of silica from a solution of ethanol, water, and ammonia. Van Tendeloo and co-workers proposed that these particles form by epitaxial growth of cylindrical assemblies from the facets of *Ia3d* cubic (MCM-48) seeds. [*J. Phys. Condens. Matter* **2003**, *15*, S3037.] Here, we reexamine this hypothesis by detailed characterization of intermediate and final mesoporous silica particles formed from ethanol/water/ammonia solutions. We find that the presence of a cubic core is not required to explain the synthesis of spherical particles with radially oriented pores. Instead, we hypothesize that the radial orientation originates at the particle surface because of the preferred alignment of CTAB micelles normal to that interface. Consistent with previous studies of the Stöber process, we initially observe small, irregular silica/surfactant clusters. After an induction time, these clusters suddenly form spherical particles larger than 100 nm in diameter because of aggregation or collapse of weakly bound clusters. No ordered micellar structure forms initially, but shortly after the appearance of large spherical particles, cylindrical surfactant micelles appear and align perpendicular to the particle/solution interface. The micelles appear to maintain their alignment normal to the interface even during particle coalescence, supporting the idea that radial orientation originates at the surface rather than the interior of the particles. A study of particles formed with varying amounts of ethanol suggests that ethanol acts as a cosolvent and as a low-dielectric constant solvent to induce cooperative effects on micelle organization and particle morphology, leading to particles with radially oriented pores at a large ethanol concentration.

Introduction

The Stöber process for the synthesis of colloidal silica has been known to the materials synthesis community for decades.¹ In this process, tetraethoxysilane is hydrolyzed in ethanol/water/ammonia solution, and uniformly sized (essentially monodisperse) particles form by precipitation. Grün et al. carried out the same process in the presence of surfactant pore templates to synthesize spherical mesoporous silica particles.^{2,3} Shortly thereafter, several groups reported that in addition to being organized into periodic arrays,^{2,3} the pores in these materials are often oriented radially toward the edges of the particles.^{4,5} This is an ideal pore arrangement for providing accessibility to the interior of the particles for applications such as catalysis and selective adsorption. Despite the potential applications, the mechanism of forming such an unusual structure is difficult to explain.

Prior studies of mesoporous materials synthesis mechanisms focused mainly on how long-range order develops and led to the conclusion that the synthesis most likely occurs through cooperative assembly of silicate species and surfactants^{6,7} driven by Coulombic⁸ or hydrogen bonding⁹ interactions. Recent studies indicate that under acidic conditions, phase separation occurs prior to the onset of long-range ordering and that this phase separation influences particle morphology.^{10–12} Contrasting this, in NaOH solution, Regev used cryo-TEM to observe elongated cylindrical micelles early in reaction, which are more

consistent with organized structure formation prior to precipitation.¹³ A TEM investigation of acid-neutralized samples suggested the opposite; in NaOH solutions, disordered aggregates form first and subsequently rearrange into ordered structures.¹⁴ However, none of these studies directly addresses Stöber synthesis conditions, and they do not explain how a radial pore orientation emerges in the presence of ethanol and ammonia.

The mechanism of morphology development in the Stöber process (in the absence of surfactants) has been studied in detail.^{15–23} Matsoukas and Gulari attributed the formation of uniform particles to fast nucleation followed by growth by monomer addition.^{15,16} Subsequent research indicated that this process is better modeled by the combination of an initial nucleation and aggregation mechanism (as originally proposed by Bogush and Zukoski)¹⁸ that may be followed by monomer or small particle addition.^{20,22} When surfactants are added to the Stöber process, the relative importance of nucleation, aggregation, and growth to the co-assembly of surfactant/silica aggregates again comes into question. Van Tendeloo et al. have proposed that the formation of radially oriented close-packed cylindrical pores can be explained by nucleation and growth.^{24,25} They suggested that a faceted *Ia3d* cubic (similar to MCM-48²⁶) aggregate forms early in the precipitation process. They proposed that hexagonally patterned silica/surfactant aggregates grow on the facets of the cubic seed to create a particle with an MCM-48 core from which cylindrical pores emanate.^{24,25}

When we attempted to apply this hypothesis to materials synthesized using the cationic fluorinated surfactant 1H, 1H,

* To whom correspondence should be addressed. E-mail: srnkink@engr.uky.edu; telephone: (859)257-9799.

2H, 2H-perfluorodecylpyridinium chloride (HFDePC) as a pore template in the presence of ethanol and ammonia, we found a conflict. The synthesized material has an X-ray diffraction (XRD) pattern indicating a 2D hexagonal close-packed (HCP) pore arrangement, and it consists of spherical particles with radially oriented pores.²⁷ However, the core region observed by TEM is very small and shows no indication of cubic ordering. This is consistent with the behavior of the surfactant; HFDePC does not form an *Ia3d* cubic phase because of the stiffness of the fluorinated chains.^{28,29} However, HFDePC may assemble in an unusual way, so here we address the following issues for the surfactant for which these radially oriented pore structures were originally discovered, cetyltrimethylammonium bromide (CTAB):

1. Is the MCM-48 core model applicable to all spherical silica particles with radial pores?
2. If the MCM-48 core model does not apply to all particles, what is actually at the center of these particles? Is it a single aggregate, a cluster of aggregates, or nonporous silica?
3. Is there evidence for MCM-48 particles early in reaction that would serve as seeds? Whether or not the seeds exist, how are the formation of spherical particles and the development of pore structure related?
4. The MCM-48 core model implies that ethanol works as a cosurfactant to induce the structure transformation from hexagonal to cubic.³⁰ However, ethanol also serves as a cosolvent for CTAB.³¹ What is the actual role of ethanol in this case, and how does it affect the pore size and pore structure?

In this paper, we will address these questions by detailed characterization of intermediate and final products of tetraethoxysilane (TEOS) hydrolysis in solutions of water, ethanol, ammonia, and CTAB. As we will show, our conclusions do not support the seeded growth mechanism proposed by Van Tendeloo et al.²⁴ We will propose an alternative hypothesis that radial pore orientation originates at the surface of malleable particles. This mechanism is more consistent with the established role of aggregation in Stöber particle synthesis.^{18,20,22} Also, while ammonia has been described as the morphology catalyst in the Stöber process,¹ a polar solvent such as ethanol also plays an important role in forming spherical particles.³² The roles of ethanol in mesoporous silica synthesis have been in dispute for some time.^{30,31,33,34} Roles as both cosolvent and cosurfactant have been suggested.^{30,31,35,36} Our results will be shown to be consistent with roles as a low-dielectric solvent and as a cosolvent for CTAB. We will discuss how these roles influence pore order and particle morphology.

Experimental Methods

Samples were prepared on the basis of the procedure of Liu et al.³⁰ The initial reactants had the molar ratios 1 TEOS:0.3 CTAB:11 NH₃:*x* C₂H₅OH:144 H₂O with *x* = 0, 10, 20, 40, or 58. The products will be called SP1 through SP5 corresponding to the order from *x* = 0 to *x* = 58. Particles were formed by mixing all reagents in the reverse order listed. The TEOS was added slowly over 1 min. After aging the solutions for 2 h at room temperature, white powder precipitates were filtered and washed with deionized water. Dried samples were calcined at 500 °C for 4 h or twice extracted with acidic ethanol (150 mL ethanol with 3 mL of concentrated aqueous HCl) to remove the surfactant.

X-ray diffraction (XRD) patterns were recorded on a Siemens 5000 diffractometer using Cu K α radiation (λ = 1.54098 Å) and a graphite monochromator. Diffraction data were recorded at 2θ values between 1.8° and 7.0° with a step size of 0.02°

and a scanning rate of 0.1 deg/min. Transmission electron microscope (TEM) images were collected with a JEOL 2010F instrument operating at 200 kV. Solidified samples were dispersed in an acetone solution and then deposited on lacey carbon grids. Nitrogen sorption measurements were performed on a Micromeritics Tristar 3000 system. All samples were degassed at 150 °C for 4 h under flowing nitrogen prior to measurement. The BJH method with a modified statistical film thickness equation³⁷ was used to calculate the pore size distributions from the adsorption branch of the isotherms.

In addition to the fully cured samples, a series of samples were prepared for TEM by cold drying, to investigate the development of particle morphology and pore structure. In this method, a lacey carbon grid was placed on a tissue and precooled to -2 ± 2 °C with liquid nitrogen. The conditions were the same as for sample SP5, except that the TEOS was added all at once. A drop of solution was quickly removed from a reacting mixture at a certain time and dropped onto the grid. The solution was quickly cooled on the grid, and simultaneously solvent was drawn away by the tissue. While the thinned layer of solution remaining on the grid was still cool, the grid was quickly blown dry with forced air at room temperature. The dried sample was examined by TEM within 4 h.

Results and Discussion

A seeded growth mechanism for spherical particles with radial pores was proposed by Van Tendeloo et al.^{24,25} However, four questions related to this mechanism still need to be addressed, as outlined in the Introduction. The discussion of our results will be organized to address those issues sequentially.

1. Are MCM-48 Cores Necessary? As discussed in the Introduction, we observed radial pores without an MCM-48 core when the fluorinated surfactant HFDePC was used.²⁷ With the doubt raised by this observation, we started to look at the structure of CTAB-templated particles in detail. We reproduced the spherical silica particle (SSP) sample of Van Tendeloo et al.²⁴ (which we call sample SP5) and examined the pore structure by TEM. We did not find evidence for MCM-48 cores in the particles that we examined. For example, a hexagonal pattern is clearly seen in the center area of the particle in Figure 1a. After tilting this particle by 10° (Figure 1b), part of the hexagonal pattern has changed to a layered pattern which is consistent with a side view of cylindrical pores rather than an MCM-48 structure. The layers are arranged in random directions in the middle of the particle which indicates that the center of the particle contains a cluster of aggregates instead of a single aggregate. Otherwise, all of the layers should be oriented in one direction. Thus, we find that at least some of the particles that have radially oriented pores do not show evidence for an MCM-48 core.

A cluster of randomly oriented cylindrical aggregates such as in Figure 1 can give rise to Moiré patterns in TEM, including both hexagonal and square dot patterns. It is conceivable that the evidence for projections of a cubic core observed previously^{24,25} was actually due to overlapping of two or more layered cylinders patterns. Because TEM has a very large depth of field, it is difficult to rule out overlapping cylinder projections. However, we have no reason to doubt the structure assignment of the sample examined by Van Tendeloo et al. We can only say that for a sample prepared under the same conditions, we found many particles that do not have the appropriate relationship of pore projections necessary to identify an MCM-48 core. Therefore, we conclude that in both HFDePC and CTAB templated particles, an MCM-48 core is not necessary for the observation of radially oriented mesopores.

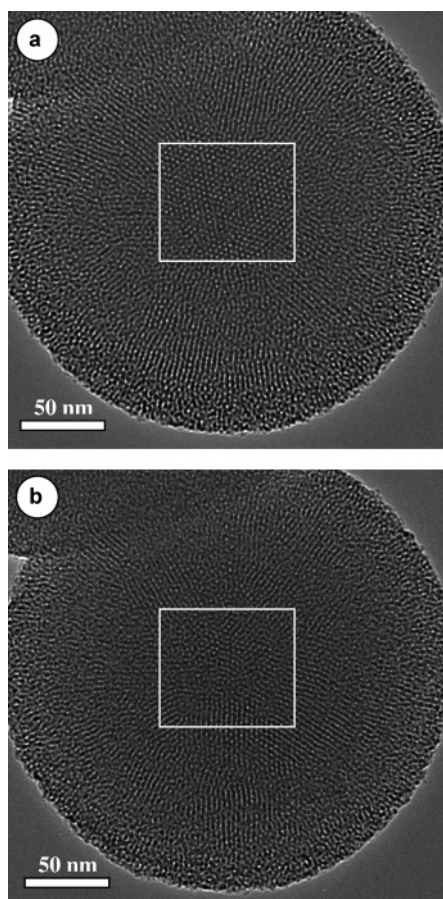


Figure 1. TEM images of the same particle from sample SP5 tilted (a) at 0° and (b) at 10°. The same region is boxed in both images.

2. What Is at the Center of the Particles? Given that MCM-48 cores are not essential for radial pore formation, we address whether there is any special “core” structure with a density differing from a “shell” on the outside of the particle. An *Ia3d* cubic structure would be expected to have a different overall density than an HCP structure. Therefore, our SP5 sample was studied with mapping by energy-dispersive X-ray spectroscopy. The result is shown in Figure 2. Figure 2a shows a dark-field scanning TEM (STEM) image and Figure 2b shows the map of integrated density of silicon and oxygen along a slice through the center of the particle. If the particle has a core of differing density, there should be a density jump at the center of the particles, similar to the decrease observed for particles with hollow cores.³⁸ If it is a uniform solid, each elemental density profile should be a smooth half-ellipse. The curves in Figure 2b conform to a smooth half-ellipse, showing that there is no special core of significantly higher or lower density than the rest of the particles with radial pores. We therefore doubt not just that there is an MCM-48 core, but that there is any type of special core structure in these particles. We suspect, as mentioned above, that the appearance of a core is more the result of observing several randomly oriented domains at the center of the particle but only one orientation near the edges. Even in a perfectly radial structure, the illusion of a core can be created by seeing projections along the pore direction at the center of the particle but across the pores near the edge of the particle.

3. Are Cubic Seeds Formed Early in Reaction? While we did not find universal evidence for the presence of cubic cores in the SP5 sample, it is still possible that despite extensive searching, we failed to find properly oriented cubic cores. Therefore, to directly test the hypothesis that cubic seeds act as

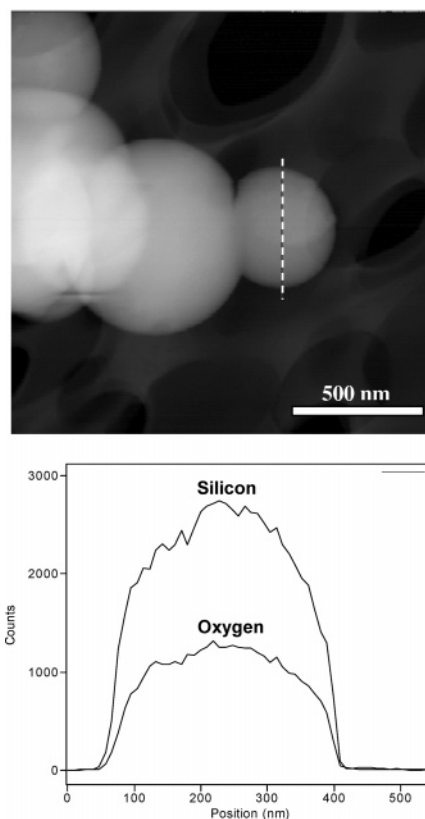


Figure 2. Density profiles of a particle from sample SP5: (a) Dark-field STEM and (b) EDS map of silicon and oxygen along the slice indicated by the dashed line.

cores, we examine cold-dried TEM samples withdrawn from the earliest possible time until radial micelles could be observed. If cubic seeds are part of the process of forming particles with radial pores, we expect to be able to isolate small MCM-48 particles.

Generally, there are two methods that have been used for the preparation of quenched reacting colloidal samples for TEM. In the first, cryo-TEM, one vitrifies the sample in liquid ethane and then observes the sample at liquid nitrogen temperature. Soft, fragile assemblies such as fractal aggregates¹⁹ and surfactant aggregates³⁹ can be captured and observed if this method is scrupulously applied. However, sample preparation is relatively slow (requiring liquid film thinning before vitrification), and samples prepared in this method cannot withstand a high-energy electron beam.⁴⁰ Therefore, it would be difficult to trace surfactant–silica aggregate formation over a few dozen seconds with this method. The second method is the drying method. In this method, researchers normally remove a liquid sample and blot it with a tissue and then let the sample dry in air.¹⁹ This method is very simple and the sample prepared is stable enough to observe surfactant/silica aggregates with a high-energy beam.^{12,14} The disadvantage is that reaction may continue to happen as the sample is dried on the grid. Fragile structures may also collapse during drying. Bearing in mind these limitations, we use the cold-drying method described above to reduce the possibility of continued silica reaction during sample preparation. The combination of cooling, blotting, and forced convection during drying should reduce artifacts, but the main artifact should be a greater density in the dried samples than in the structures present in solution.¹⁹ In particles withdrawn during the Stöber process, Bailey and Mecartney found that drying produced dense particles with fuzzy edges early in reaction because of the collapse of ramified, weakly condensed silica

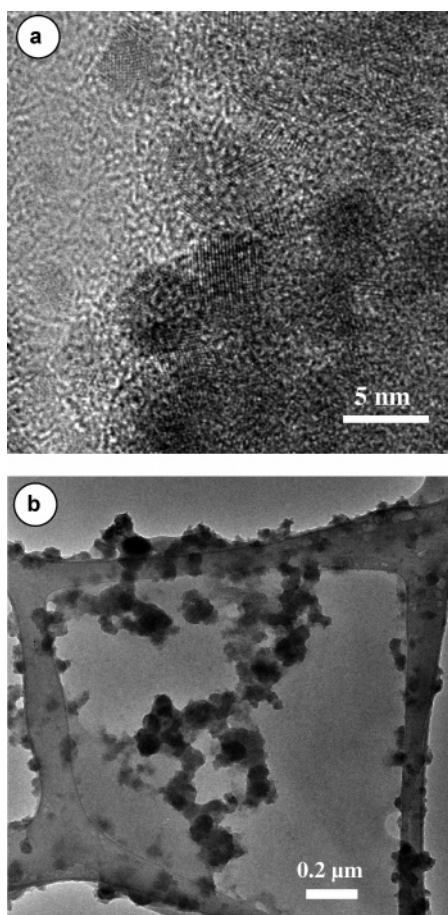


Figure 3. TEM images of cold-dried samples withdrawn at early stages of the synthesis of sample SP5 after (a) 10 s and (b) 50 s. The fringe patterns in image (a) come from crystallized CTAB clusters.

clusters that could be observed by cryo-TEM.¹⁹ The dense, smooth spherical particles found at later stages of reaction looked similar by cryo-TEM or drying.¹⁹

To search for cubic seed particles, we study samples withdrawn during a synthesis batch of sample SP5. Samples were removed every 10 s until 90 s elapsed. The synthesis solution became turbid approximately 60 s after the addition of TEOS. Representative TEM images are shown in Figures 3–5. After 10–20 s, only weakly condensed, amorphous silica/CTAB aggregates with ill-defined structures are observed (not shown). The images appear to be made up of small (4–8 nm) dark spots uniformly suspended in a gray matrix. At high magnification (Figure 3a), the dark spots give fringe patterns indicating that they are atomically crystalline. Because the silica does not crystallize under these conditions, we interpret these spots as being CTAB aggregates (micelles or microcrystals). The sizes of these clusters are consistent with the sizes of CTAB micelles observed in solution by cryo-TEM³⁹ and dynamic light scattering.⁴¹ In Figure 3a, we can see that these clusters are suspended in an amorphous matrix of silica.

After 50 s of reaction, more distinct particles with rough edges are observed (Figure 3b). The structures of these particles are similar to the structures observed in dried Stöber samples early in reaction by Bailey and Mecartney.¹⁹ We cannot be sure of the precise nature of the aggregates in solution, but the appearance of these particles may be due to the collapse of weakly condensed silica/surfactant aggregates with ramified structures. From statistical analysis of a set of randomly selected particles, the size of the dried aggregates is around 50 nm and the standard deviation of the sample is 15 nm. At higher magnification (not

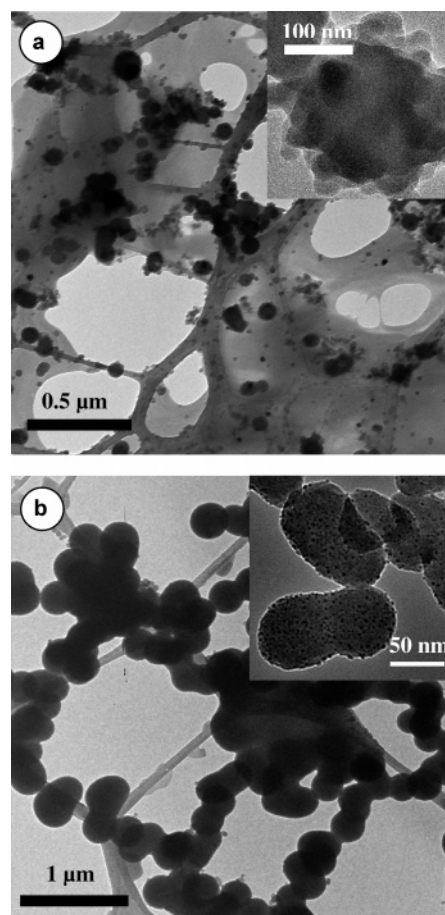


Figure 4. TEM images of cold-dried samples withdrawn at intermediate stages of the synthesis of sample SP5 after (a) 60 s and (b) 70 s.

shown), CTAB micelles are still observed throughout the particles, which show no sign of any long-range order.

After 60 s of reaction, a new stage begins which is marked by the onset of turbidity. At this point, a bimodal distribution of particles is observed in the dried TEM sample (Figure 4a). The smaller particles are 24 ± 4 nm in diameter, and the large ones are 90 ± 23 nm. The smooth edges of the majority of the particles suggest that they did not collapse during the drying process of sample preparation. If they were, rough edges should be observed.⁴⁰ However, some rough particles are still rarely observed, and their raspberry-like appearance (inset of Figure 4a) suggests that large particles form by aggregation of several smaller clusters. Although spherical particles with sizes comparable to the final particle size begin to appear this time, no ordered surfactant aggregates can be found in any of the particles.

At 70 s, the sample consists mainly of large spherical particles with diameters in the range of 350 ± 30 nm (Figure 4b). A smaller number of small (41 ± 7 nm) particles are also present, but they also have smooth edges (inset of Figure 4b). CTAB micelles are still present, but now they appear to coat the particles (the dark spots in the inset of Figure 4b). The coating of micelles probably was not deposited during drying, because if it were, we would anticipate a uniform coating of the crystals all over the grid, which is not observed. These crystals indicate that the positively charged surfactant micelles might be attracted to surround the negatively charged silica/surfactant particles in the synthesis solution. Also at 70 s, ordered patterns start to be apparent for some of the particles, but they are not shown

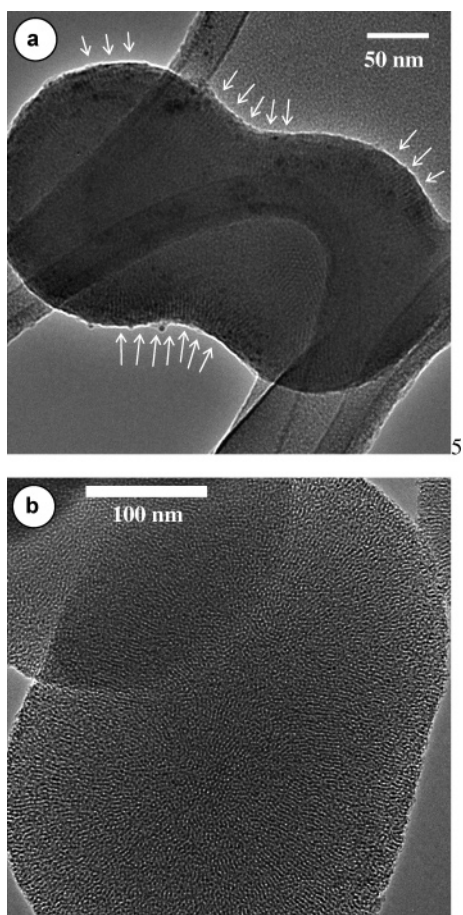
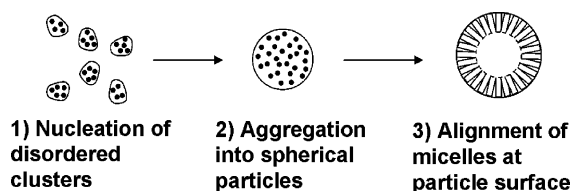


Figure 5. TEM images of anisotropic particles found in the SP5 synthesis solution (a) cold-dried after 90 s and (b) filtered and calcined after 2 h of aging. Arrows indicate the orientation of micelles at the interface of the particles.

because of poor contrast. This is consistent with the findings in acidic conditions and in acid-quenched NaOH solutions of initially amorphous silica/surfactant aggregates that order upon aging.¹²

Ordered patterns were clearly visible in many particles for the sample collected at 90 s. Figure 5a shows a particle with peanut shape and stripe features along its edge. The dark stripes are CTAB micelles. This particle is not representative of the particle shapes in this sample; many spherical particles were also observed in samples removed and dried at this time. However, there are also many particles with shapes, such as this peanut shape, that appear to have formed by aggregation of two or more spherical particles. If the mechanism were nucleation and growth by monomer addition, then all particles would be expected to be spherical since the rate of growth should be the same in all directions. The stripes at the edges of the particles are surprising because they are always oriented perpendicular to the edge. A similar pore structure was also identified in the calcined sample SP5a obtained by adding the TEOS precursor to the synthesis solution all at once and aging for 2 h. Figure 5b shows a peanut-shaped particle that was isolated from this sample, which has mesopore channels arranged perpendicular to its edge. This calcined sample also contains many spherical particles with radially oriented pores. This suggests that during the process of aggregation and particle reformation, the micelles are able to reorient such that they always stay perpendicular to the edges of the particles. This would be very difficult to explain in terms of an Ostwald ripening mechanism or a monomer addition mechanism, and

SCHEME 1^a



^a The proposed mechanism of forming spherical silica with radial mesopores with a high concentration of ethanol. Nucleation begins with small disordered clusters which aggregate into large particles, followed by micelle organization at the particle surface.

we instead propose that the “large” (> 100 nm) particles formed at the onset of turbidity are still liquidlike. They are disordered immediately after precipitation and ordered structures form only in the concentrated silicate/surfactant phase. We find no evidence for any MCM-48 cubic silica particles prior to or after the formation of the radially oriented micelles.

Particle size distributions of the samples collected at 60, 70, and 90 s have two distinct maxima: one ≥ 100 nm and the other < 100 nm. There are few particles with intermediate sizes. The smaller particles may come from the collapse of ramified low-density structures during the synthesis process as suggested by Bailey et al.¹⁹ The bimodal particle size distribution indicates that the smaller particles do not simply grow by monomer addition after the collapse of the low-density clusters. Instead, these clusters must aggregate together to form denser and larger particles or aggregate with existing large, dense particles. The absence of particles with intermediate sizes supports the role of aggregation. Preferential aggregation of small particles with large ones is predicted by DLVO theory and is consistent with previous observations of the Stöber process.²²

The mechanism of the Stöber process with a cationic surfactant template suggested by these TEM observations is summarized in Scheme 1 and can be described as follows. At first, silica/surfactant clusters form and may be weakly connected into low-density aggregates. These clusters become larger and denser as silica species continue to be generated by hydrolysis. When a large number of clusters of sufficient size is present in solution, they become colloiddally unstable and suddenly collapse or aggregate together to form large denser spherical particles and the solution becomes turbid. The negatively charged particles may continue to attract positively charged CTA⁺ micelles which surround the particles, and small clusters (already present or newly nucleated) may add to the surface of these particles. After these large spherical particles have formed, the surfactants organize into cylindrical micelles and form a close-packed layer aligned perpendicular to the outer edge of the particle. As particles aggregate together, and as they continue to grow, this perpendicular alignment is maintained. When the particles are still soft, this alignment should be thermodynamically driven by the preferential orientation of the micelles at the interface. The exact reason for this orientation is not known, but it may be due to the interface between the silica/surfactant phase and the mixed ethanol/water solvent being equally attractive toward polar and nonpolar species. Monte Carlo simulations have shown that interfaces that interact equally with polar or nonpolar species induce perpendicular alignment of nonionic surfactant mesophases.⁴² It is possible that the particles can then continue to grow by epitaxial growth of silica/CTAB clusters at the radially patterned particle surface. This mechanism suggests that if the particles vitrify too quickly, it may not be possible for the micelles to adopt their preferred

orientation normal to the interface, which explains why these radial structures are not always seen.⁵

4. What is the Role of Ethanol in Determining Pore Structure and Orientation? Part of the explanation for the feasibility of an MCM-48 core in silica spheres with radial pores was that, by acting as a cosurfactant, ethanol induces a hexagonal-to-cubic transformation, leading to the cubic seeds from which radii emanate. Finding little support above for the necessity of an MCM-48 core in radially oriented silica particles, we also question the role of ethanol as a cosurfactant. There is little support for this idea in the surface science literature.

Roles of ethanol as both cosolvent and cosurfactant for CTAB have been cited by researchers making mesoporous silica.^{30,31,35} If ethanol works as cosurfactant, it has been suggested that it will swell the palisade layer and increase the diameter of the micelles (and therefore of the pores in the material).^{30,36} If it acts as cosolvent, it will reduce the micelle (pore) sizes by decreasing the aggregation number.³¹ In either case, the change of micelle size should be reflected in the pore size of the product.⁵ To examine this change, we prepared a series of samples (SP1–5) with all parameters fixed but an increasing amount of ethanol. This series reproduces the series of Liu et al.³⁰ and was subject to detailed characterization.

The XRD patterns of the calcined samples SP1, SP3, and SP5 are similar to what was reported by Liu et al. as samples E0, E20, and E58.³⁰ Samples SP1 and SP2 display three peaks indexed to a 2D HCP structure. Sample SP3 displays an *Ia3d* cubic structure, perhaps mixed with a minority of HCP structure. Sample SP5 has a 2D HCP pattern with broad peaks. However, sample SP4 is different than the (supposedly identical) sample E40 of Liu et al. Both the as-synthesized and calcined XRD patterns (Figure 6a) show that SP4 consists primarily of HCP structures, with perhaps a minority of cubic phase indicated by the weak shoulder to the right of the (100) reflection. No cubic–lamellar structure such as the one described by Liu et al. was identified between the cubic (SP3) and hexagonal (SP5) structures.³⁰ In fact, we saw some deterioration of the cubic structure in sample SP4 in favor of the HCP structure upon calcination, rather than loss of a “lamellar” structure in favor of a cubic structure. The difference between our samples and those of Liu et al. may be due to subtle differences in the aging and drying steps (which were not fully described).³⁰ In our samples, we find that as the ethanol content increases, the pore structure in the SP series transforms from hexagonal (SP1/2) to cubic (SP3) and back to hexagonal (SP4/5).

TEM images were collected for this series to confirm the conclusions from XRD patterns and to trace the transformation of the particle morphology. With increasing ethanol, we observe not only a pore structure transformation from hexagonal to cubic to hexagonal, but also a particle morphology change from irregular to elongated to spherical. SP1 consists only of rough irregular particles. SP2 is made up of elongated cylindrical particles with cylindrical pores running parallel to the main axis of the particles (previously described as a tube-within-a-tube structure).³⁶ SP3 contains both spherical and (American) football-like particles. Many of the particles are faceted, and projections corresponding to views of an *Ia3d* cubic structure are evident, consistent with the characterization of Liu et al.³⁰ Both SP4 (Figure 6b) and SP5 (Figure 1) consist of almost perfectly spherical, uniform particles. Some of the pores in SP4 are arranged radially while others are arranged randomly. The structure of SP4 again casts doubt on the assumption of the need for an MCM-48 core to explain the formation of radial pores. Even though the XRD pattern of SP4 is very similar to

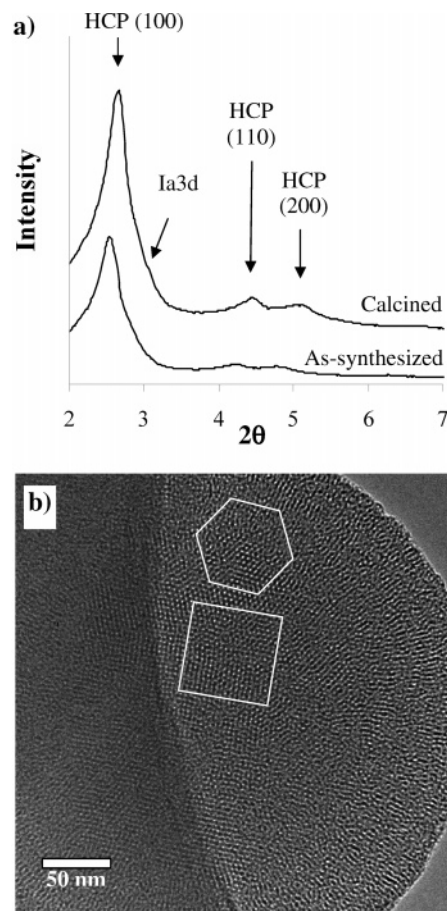


Figure 6. Characterization of sample SP4: (a) XRD patterns of as-synthesized and calcined materials and (b) TEM image of calcined sample. The hexagon outlines a hexagonal close-packed region and the square outlines a square close-packed region (associated with an *Ia3d* cubic crystallite).

what has been described by Van Tendeloo et al. for an ideal sample with radial pores,²⁴ the TEM images are more consistent with a mixed polycrystalline structure than with MCM-48 cores and HCP shells. Figure 6b shows both hexagonal and square pore arrays, neither located at the center of the particle. We could not precisely confirm that the square pore array is from an *Ia3d* cubic structure, but whether it is from a cubic domain or a Moiré pattern from HCP domains, it shows that randomly oriented domains form during the precipitation process rather than one phase serving as a nucleus for the other.

Figure 7 shows a comparison of the pore size distributions of samples SP1, SP2, SP4, and SP5, all of which have primarily HCP pore structures. The pore sizes of SP2, SP4, and SP5 are all the same and are slightly smaller than the pore size of SP1. This change is most consistent with ethanol acting as a cosolvent for CTAB in this case. The trend is not consistent with the cosurfactant role proposed by Liu et al.³⁰

The observations for the SP1–5 series can be better explained in terms of ethanol’s roles as low-dielectric solvent and as a cosolvent for CTAB. A limited amount of ethanol (up to ~2.4 mol/L) decreases the critical micelle concentration (cmc) of CTAB.⁴³ However, short-chain alcohols such as ethanol and propanol go to the palisade region of CTAB micelles rather than acting as true cosurfactants.^{43,44} This lowers the dielectric constant for interactions between headgroups and lowers the micelle aggregation number.⁴³ At the same time, the fraction of ionized (dissociated) micelle headgroups increases.⁴³

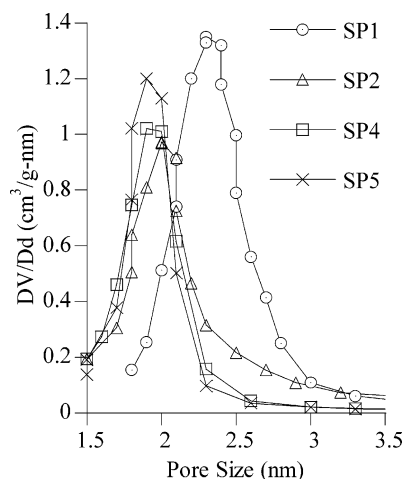


Figure 7. BJH pore size distributions of samples SP1, SP2, SP4, and SP5 from nitrogen adsorption isotherms.

At higher concentrations (above 2.4 mol/L), ethanol acts as a cosolvent and increases the cmc of CTAB as it is added.^{43,45} The ethanol decreases the hydrophobic force that drives micelle formation, which we expect to first decrease the size of the micelles and eventually to decrease their number. At the same time, the dielectric constant of the continuous solvent phase decreases as ethanol is added, which should increase the extent of counterion association. This should lead to a decrease in the surface area per surfactant in the aggregates and therefore favor low-curvature aggregates such as cylindrical micelles and bilayers.⁴⁶ Consistent with this, as ethanol is added to a hexagonal CTAB mesophase, the unit cell size decreases because of a decrease in the surfactant aggregation number.⁴⁷ However, at high concentration, the cosolvent effect destroys the long-range ordering, and only micellar solutions are observed.⁴⁷

Taking into account all of the observations of the effects of ethanol addition to aqueous CTAB solutions, we can explain the trends that are observed in materials synthesis. The sample with no ethanol present initially (SP1) actually contains a significant amount of ethanol because of TEOS hydrolysis. At least one mole is generated per mole of TEOS (corresponding to 0.33 mol/L ethanol) and as much as 1.3 mol/L may be present by the end of the reaction. These concentrations are in the range where ethanol decreases the cmc by partitioning into the palisade layer of the micelles, at the same time increasing the dissociation of counterions from the micelle surface.⁴³ Because of good dissociation, the silicate ions generated by hydrolysis remain soluble in solution for a relatively long time, and they co-assemble with the micelles after a significant amount of condensation has occurred. The co-assembly leads to a hexagonal phase but with randomly oriented domains and irregular particle morphology.

The first sample with added ethanol (SP2) contains almost 3 mol/L of ethanol at the beginning and may contain as much as 3.9 mol/L by the end of the hydrolysis reaction. This is well above the concentration where ethanol begins to act as a cosolvent and begins to increase the cmc of CTAB.⁴³ We expect the dielectric constant of the mixed solvent to have decreased in this solution, promoting more ion association between the headgroups and counterions. This means that the headgroups will not be as charged and therefore will be better able to assemble into low-curvature structures (cylindrical micelles). The high degree of association should also mean that the silicate species begins to interact with the micelles sooner in the

synthesis process. This may slow their rate of condensation and allow long, well-organized close-packed micelle structures to form, which result in elongated particles. Despite a larger degree of silica–surfactant association, the silica:surfactant ratio may decrease because of preferential association of bromide with CTAB.⁴⁸ The pore size of the product decreases, which is consistent with the lower aggregation numbers observed for CTAB micelles and hexagonal phases as ethanol is added.^{43,47}

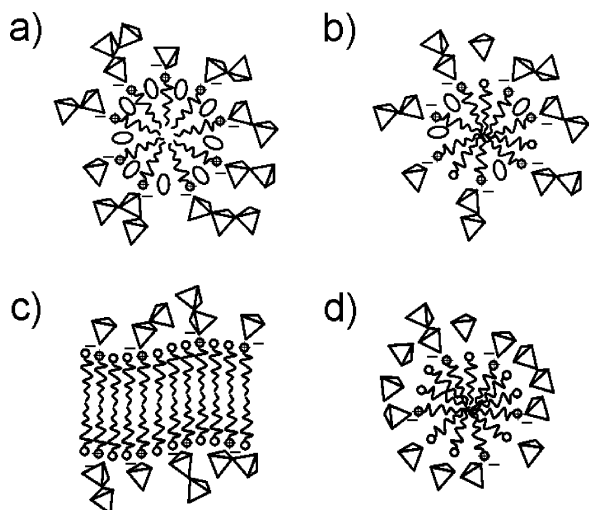
With more ethanol (SP3), we expect the micelle aggregation number to decrease and the degree of ion association to increase. This decreases the driving force for co-assembly of the silicates with surfactants and therefore should lower the silica:surfactant ratio in the product. This decreases the headgroup area in the resulting product, which explains the transition from the 2D HCP to the *Ia3d* cubic structure.

When still more ethanol is added (samples SP4 and SP5), a transition is seen back from the *Ia3d* cubic structure to a 2D HCP structure. This is difficult to explain in terms of the known cosolvent and dielectric effects of ethanol. It may be that the decline in the number of micelles is large enough that the silica:surfactant ratio in the co-assembled product starts to increase compared to sample SP3. This may not be the only explanation, since the TEM images in Figures 3–5 suggest that phase separation happens early in the particle synthesis process. The spherical morphology of the particles suggests that the process may initially be liquid–liquid phase separation. Partitioning of species between solvent-rich and the silica/surfactant-rich phases may influence the type of self-assembled mesophases that forms. The silica–surfactant phase that precipitates from these solutions should be poor in ethanol, which would promote the formation of a phase more similar to a sample with a lower amount of ethanol such as SP2. Another potential factor is that as ethanol decreases the hydrophobic driving force for CTAB micellization, ammonium may become a more competitive counterion for silica anions, which would increase the silica:surfactant ratio as well. Predicting the phase behavior of such a complex mix of dynamically evolving, hydrogen bonding, and charged species is a difficult thermodynamic problem, but an increase in the silica:surfactant ratio because of the partitioning of species between solvent and silica/surfactant phases is a plausible explanation for the change from the *Ia3d* cubic to 2D HCP structure.

While the precise nature of the transition of the mesophases structure from hexagonal to cubic and back to hexagonal can only be addressed by a better understanding of silica–surfactant–solvent phase behavior, we attribute our observations to the roles of ethanol as CTAB cosolvent and low-dielectric constant solvent rather than as a cosurfactant. Scheme 2 summarizes the implications of these roles. As the ethanol content increases, the scheme reflects increasing solubility of CTAB in the continuous phase, increasing counterion association, and decreasing solubility of the silicate species in the continuous phase. The decreasing silicate solubility leads to earlier association of shorter silicate oligomers with the surfactant. The observation of a similar effect of methanol on the pore structure transitions (from hexagonal to cubic to hexagonal)³⁰ supports this interpretation.

Conclusions

In this study, we directly investigated the mechanism of forming silica spherical particles with radially orientated mesopores. We examined both intermediate and final products formed during precipitation of silica and CTAB from solutions of ethanol, water, and ammonia. We found no support for the

SCHEME 2^a

^a Proposed local effect of ethanol on the silicon (tetrahedra):surfactant ratio and the micelle structure: (a) with only the ethanol (ellipsoids) generated by hydrolysis, (b) with a small amount of ethanol added, (c) with a moderate amount of ethanol added, and (d) with a large amount of ethanol added. Headgroup and silicate charges are indicated. Absence of a charge indicates an uncharged species or counterion association.

hypothesis that *la3d* cubic particles form initially and act as seeds for the growth of radially oriented pores. We proposed an alternative explanation for the formation of these spherical particles that is more consistent with prior investigations of the Stöber process. Our hypothesis, supported by products isolated during the particle synthesis, is that particles form by nucleation of silica/surfactant clusters which aggregate into spherical particles. The radial orientation of the pores emerges because of the alignment of CTAB micelles at the interface between the solvent and malleable silica/surfactant aggregates. We also found support for roles of ethanol as a CTAB cosolvent and a low-dielectric constant medium. The transform of the pore structure from hexagonal to cubic and back to hexagonal with increasing ethanol content can be related to changes in the silica:surfactant ratio. Ethanol also influences the particle morphology by influencing the relative rates of precipitation, condensation, and co-assembly of the particles. By promoting association between less condensed silicate species and surfactants, ethanol induces a morphological transformation from irregular particles to weakly faceted particles (elongated or cubic) to spherical particles. We hope that these hypotheses will inspire further theoretical and in-situ experimental investigations of the synthesis of these materials.

Acknowledgment. The authors thank Dr. Alan Dozier for help with the STEM and EDS experiments. This work is based upon work partially supported by the National Science Foundation under grant no. DMR-0210517. B.T. was supported by a Kentucky Research Challenge Trust Fund graduate fellowship.

References and Notes

- (1) Stöber, W.; Fink, A. *J. Colloid Interface Sci.* **1968**, *26*, 62.
- (2) Grün, M.; Lauer, I.; Unger, K. K. *Adv. Mater.* **1997**, *9*, 254.
- (3) Grün, M.; Unger, K. K.; Matsumoto, A.; Tsutsumi, K. *Microporous Mesoporous Mater.* **1999**, *27*, 207.
- (4) Pauwels, B.; Van Tendeloo, G.; Thoelen, C.; Van Rhijn, W.; Jacobs, P. A. *Adv. Mater.* **2001**, *13*, 1317.
- (5) Nooney, R. I.; Thirunavukkarasu, D.; Chen, Y.; Josephs, R.; Ostafin, A. E. *Chem. Mater.* **2002**, *14*, 4721.
- (6) Chen, C.-Y.; Burkett, S. L.; Li, H.-X.; Davis, M. E. *Microporous Mater.* **1993**, *2*, 27.
- (7) Firouzi, A.; Kumar, D.; Bull, L. M.; Besier, T.; Sieger, P.; Huo, Q.; Walker, S. A.; Zasadzinski, J. A.; Glinka, C.; Nicol, J.; Margolese, D.; Stucky, G. D.; Chmelka, B. F. *Science* **1995**, *267*, 1138.
- (8) Huo, Q. S.; Margolese, D. I.; Ciesla, U.; Feng, P. Y.; Gier, T. E.; Sieger, P.; Leon, R.; Petroff, P. M.; Schüth, F.; Stucky, G. D. *Nature* **1994**, *368*, 317.
- (9) Tanev, P. T.; Pinnavaia, T. J. *Science* **1995**, *267*, 865.
- (10) Chan, H. B. S.; Budd, P. M.; Naylor, T. d. *J. Mater. Chem.* **2001**, *11*, 951.
- (11) Yu, C.; Fan, J.; Tian, B.; Zhao, D. *Chem. Mater.* **2004**, *16*, 889.
- (12) Flodström, K.; Wennerström, H.; Alfredsson, V. *Langmuir* **2004**, *20*, 680.
- (13) Regev, O. *Langmuir* **1996**, *12*, 4940.
- (14) Sadasivan, S.; Fowler, C. E.; Khushalani, D.; Mann, S. *Angew. Chem., Int. Ed.* **2002**, *41*, 2151.
- (15) Matsoukas, T.; Gulari, E. *J. Colloid Interface Sci.* **1989**, *132*, 13.
- (16) Matsoukas, T.; Gulari, E. *J. Colloid Interface Sci.* **1991**, *145*, 557.
- (17) Bogush, G. H.; Zukoski, C. F. *J. Colloid Interface Sci.* **1991**, *142*, 1.
- (18) Bogush, G. H.; Zukoski, C. F. *J. Colloid Interface Sci.* **1991**, *142*, 19.
- (19) Bailey, J. K.; McCartney, M. L. *Colloids Surf.* **1992**, *63*, 151.
- (20) Giesche, H. J. *Eur. Ceram. Soc.* **1994**, *14*, 189.
- (21) Boukari, H.; Lin, J. S.; Harris, M. T. *J. Colloid Interface Sci.* **1997**, *194*, 311.
- (22) Lee, K.; Sathyagal, A. N.; McCormick, A. V. *Colloids Surf., A: Physicochem. Eng. Aspects* **1998**, *144*, 115.
- (23) Green, D. L.; Lin, J. S.; Lam, Y.-F.; Hu, M. Z.-C.; Schaefer, D. W.; Harris, M. T. *J. Colloid Interface Sci.* **2003**, *266*, 346.
- (24) Van Tendeloo, G.; Lebedev, O. I.; Collart, O.; Cool, P.; Vansant, E. F. *J. Phys.: Condens. Matter* **2003**, *15*, S3037.
- (25) Lebedev, O. I.; Van Tendeloo, G.; Collart, O.; Cool, P.; Vansant, E. F. *Solid State Sci.* **2004**, *6*, 489.
- (26) Beck, J. S.; Vartuli, J. C.; Roth, W. J.; Leonowicz, M. E.; Kresge, C. T.; Schmitt, K. D.; Chu, C. T. W.; Olson, D. H.; Sheppard, E. W.; McCullen, S. B.; Higgins, J. B.; Schlenker, J. L. *J. Am. Chem. Soc.* **1992**, *114*, 10834.
- (27) Tan, B.; Lehmler, H. J.; Vyas, S. M.; Knutson, B. L.; Rankin, S. E. *Chem. Mater.* **2004**, submitted.
- (28) Wang, K.; Karlsson, G.; Almgren, M.; Asakawa, T. *J. Phys. Chem. B* **1999**, *103*, 9237.
- (29) Wang, K.; Örödd, G.; Almgren, M.; Asakawa, T.; Bergenstahl, B. *Langmuir* **2000**, *16*, 1042.
- (30) Liu, S.; Cool, P.; Collart, O.; Voort, P. V. D.; Vansant, E. F.; Lebedev, O. I.; Van Tendeloo, G.; Jiang, M. J. *Phys. Chem. B* **2003**, *107*, 10405.
- (31) Anderson, M. T.; Martin, J. E.; Odinek, J. G.; Newcomer, P. P. *Chem. Mater.* **1998**, *10*, 311.
- (32) Domínguez, J. M.; Terrés, E.; Vázquez, A. *Microporous Mesoporous Mater.* **2003**, *66*, 341.
- (33) Lin, H.-P.; Mou, C.-Y. *Acc. Chem. Res.* **2002**, *35*, 927.
- (34) Walls, J. F.; Zukoski, C. F. *Langmuir* **1999**, *15*, 7432.
- (35) Lin, H.-P.; Kao, C.-P.; Mou, C.-Y. *Microporous Mesoporous Mater.* **2001**, *48*, 135.
- (36) Lin, H.-P.; Cheng, Y.-R.; Liu, S.-B.; Mou, C.-Y. *J. Mater. Chem.* **1999**, *9*, 1197.
- (37) Sayari, A.; Kruk, M.; Jaroniec, M. *Catal. Lett.* **1997**, *49*, 147.
- (38) Chen, J.-F.; Ding, H.-M.; Wang, J.-X.; Shao, L. *Biomaterials* **2004**, *25*, 723.
- (39) Vinson, P. K.; Bellare, J. R.; Davis, H. T.; Miller, W. G.; Scriven, L. E. *J. Colloid Interface Sci.* **1991**, *142*, 74.
- (40) Bailey, J. K. Direct Observation and Modeling of Microstructural Development in Chemical Processing of Ceramics. Ph.D. Thesis, University of Minnesota, Minneapolis, MN, 1991.
- (41) Dorshow, R.; Briggs, J.; Bunton, C. A.; Nicoll, D. F. *J. Phys. Chem.* **1982**, *86*, 2388.
- (42) Rankin, S. E.; Malanoski, A. P.; van Swol, F. *Mater. Res. Soc. Symp. Proc.* **2001**, *636*, 121.
- (43) Zana, R.; Yiv, S.; Strazielle, C.; Lianos, P. *J. Colloid Interface Sci.* **1981**, *80*, 208.
- (44) Jagannathan, N. R.; Venkateswaran, K.; Herring, F. G.; Patey, G. N.; Walker, D. C. *J. Phys. Chem.* **1987**, *91*, 4553.
- (45) Huang, J.-B.; Mao, M.; Zhu, B.-Y. *Colloids Surf., A: Physicochem. Eng. Aspects* **1999**, *155*, 339.
- (46) Israelachvili, J. N.; Mitchell, D. J.; Ninham, B. W. *J. Chem. Soc., Faraday Trans. 2* **1976**, *72*, 1525.
- (47) Fontell, K.; Khan, A.; Linstrom, B.; Maciejewska, D.; Puang-Hgern, S. *Colloid Polym. Sci.* **1991**, *269*, 727.
- (48) Zana, R.; Frasc, J.; Soulard, M.; Lebeau, B.; Patarin, J. *Langmuir* **1999**, *15*, 2603.